

Universal distributions of overlaps from unitary dynamics in generic quantum many-body systems

Alexios Christopoulos,¹ Amos Chan,² and Andrea De Luca¹

¹*Laboratoire de Physique Théorique et Modélisation,
CNRS UMR 8089, CY Cergy Paris Université,
F-95302 Cergy-Pontoise, France*

²*Department of Physics, Lancaster University, Lancaster LA1 4YB, United Kingdom*
(Dated: April 17, 2024)

We study the preparation of a quantum state using a circuit of depth t from a factorized state of N sites. We argue that in the appropriate scaling limit of large t and N , the overlap between states evolved under generic many-body chaotic dynamics belongs to a family of universal distribution that generalizes the celebrated Porter-Thomas distribution. This is a consequence of a mapping in the space of replicas to a model of dilute domain walls. Our result provides a rare example in which analysis at an arbitrary number of replicas is possible, giving rise to the complete overlap distribution. Our general picture is derived and corroborated by the exact solution of the random phase model and of an emergent random matrix model given by the Ginibre ensemble. Finally, numerical simulations of two distinct random circuits show excellent agreement, thereby demonstrating universality.

Introduction. — The relaxation dynamics of quantum manybody systems has received much attention in the last decades [1]. In recent years, the focus has shifted to determining the scrambling capabilities of a system with implications toward quantum chaos [2–4] and holography [5, 6]. A universal concept is based on the comparison of quantum states resulting from a dynamical process with the uniform distribution of states in a Hilbert space (Haar ensemble). This formulation leads to the notion of quantum k state design, defined as an ensemble of states capable of replicating the Haar distribution for all polynomial functions in the state, of degree at most k [7–10]. Both unitary designs (in which states are generated by applying unitary gates) [11, 12] and non-unitary ones (in which generalized quantum measurements are also considered) have been considered recently [13–16]. Understanding how many operations are needed to achieve a good quantum state design is an open question in many cases, with important applications to quantum computation, particularly benchmarking [17, 18], quantum circuit complexity [19–22], and more generally in quantum information, with a wide range reaching as far as black holes [6, 23–25]. In this regard, random unitary circuits (RUC) have served as vital constructs in quantum information and many-body physics, providing a unique model for strongly coupled dynamics and effective randomization [26]. Recent explorations involve the use of RUCs to examine operator growth [3, 27–29] and the spreading of entanglement [30–32] amid chaotic evolution, and spectral statistics [4, 33–36].

In this Letter, we deal with the problem of preparing a random quantum state using different realizations of a circuit. Assuming that the circuit acts on N q-qits and has depth t , we focus on the overlap distribution $w = \mathcal{N} |\langle \Psi | \Psi' \rangle|^2 = \mathcal{N} |\langle \Psi_0 | W'^{\dagger} W | \Psi_0 \rangle|^2$ between two such generated states, where $\mathcal{N} = q^N$ is the Hilbert

space dimension and W and W' are two independent realizations of the circuit with overall depth t with $|\Psi_0\rangle$ a factorized reference state. In the limit of large t , the circuit is expected to provide a k design for arbitrarily large k displaying the emergence of random matrices. In such a regime, the distribution $p(w)$ of w converges to the well-known Porter-Thomas (PT) distribution $p(w) \sim e^{-w}$ [37], associated with the overlap between two uniformly chosen pure states. The timescales for building a k -designs in this context have been studied in [38], where it was demonstrated that, in the limit of large local dimension, a geometrical interpretation similar to the one proposed for entanglement entropies emerges [32, 39], suggesting that RUCs form approximate unitary k designs at $t \sim O(Nk)$ depth. However, when both t and N are large, we identify a scaling regime dependent on a single parameter $x = N/N_{\text{Th}}(t)$, with a corresponding family of universal distributions $p(w; x)$, largely independent of the microscopic details. Here $N_{\text{Th}}(t)$ denotes a volume scale within which complete scrambling has occurred.

In $1 + 1$ dimensions, the universal scaling regime can be understood by noting that the overlap w naturally has the form of a two-dimensional partition function and can thus be expressed as the product of the transfer matrices in the spatial direction [Fig. 1(a)]. As discussed recently in [40], the distribution of singular values of such a matrix product can be studied in the space of replicas, leading to an effective $1D$ model with ferromagnetic interactions in the space of permutations. The PT distribution corresponds to the regime where only ferromagnetic vacua are relevant. In the scaling limit, x controls the density of diluted domain-walls excitations and universality emerges. We confirm this picture with heuristical analysis using the emergence of random matrices known as Ginibre ensemble, exact analysis of a RUC in the limit of

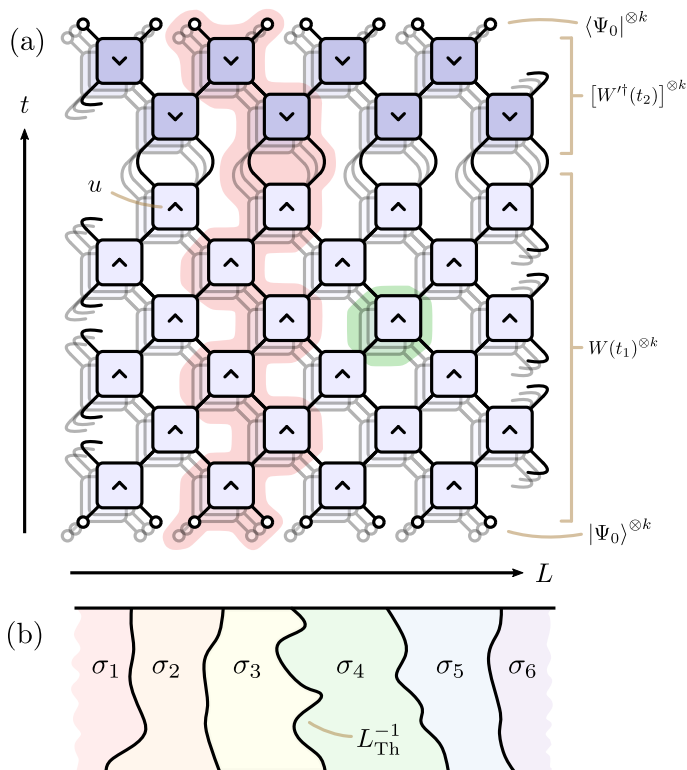


FIG. 1. (a) A representation of the overlap $w^k = \langle \Psi_0 | W^{\dagger}(t_2 = 1) W(t_1 = 3) | \Psi_0 \rangle^{\otimes k}$ with $k = 3$ for depth t and system size L . The transfer matrix is highlighted in red. The tensor product, $u \otimes u^* \otimes \dots \otimes u \otimes u^*$, is highlighted in green, which, upon ensemble-averaging, can be represented as a sum of operators of permutation states. (b) In the Thouless scaling limit, the overlap $\mathbb{E}[w^k]$ can be interpreted as the grand canonical partition function of a dilute gas of domain walls, corresponding to transpositions connecting two permutations and each carrying a fugacity L_{Th}^{-1} . Correspondingly, the size of each domain is $\sim L_{\text{Th}}(t)$.

large local Hilbert space dimension, and numerics on two distinct RUCs. We argue that the existence of a scaling limit generalizes to a spatial dimension $d > 1$. In this case, however, the excitations are identified with isolated defects in the ordered ferromagnetic sea.

Ensembles of pure states. — We define an ensemble of pure states as a distribution obtained acting on the reference $|\Psi_0\rangle$ through unitary operators W drawn from a certain measure by $\mathcal{E} := \{W | \Psi_0\rangle, W \sim d\mu(W)\}$. Given an ensemble \mathcal{E} , we further define the overlap distribution as $p_{\mathcal{E}}(w) = \mathbb{E}[\delta(w - \mathcal{N} |\langle \Psi | \Psi' \rangle|^2)]_{\mathcal{E}}$, where the average is over $|\Psi\rangle, |\Psi'\rangle$, both drawn independently from \mathcal{E} . The moments $\mathcal{N}^{-k} \mathbb{E}[w^k]_{\mathcal{E}} =: F_{\mathcal{E}}^{(k)}$ define the frame potentials. It is easily verified that the frame potentials are minimal for the uniform distribution of states, associated with the Haar ensemble $\mathcal{E}_{\text{H}} := \{U | \Psi_0\rangle \mid U \sim \text{Haar}[U(\mathcal{N})]\}$, associated with the Haar measure over the unitary group $U(\mathcal{N})$ of size \mathcal{N} [41]. In this case, one has simply $F_{\text{H}}^{(k)} = \binom{\mathcal{N}+k-1}{k}^{-1} \sim k! \mathcal{N}^{-k}$ associated to the PT dis-

tribution $p_{\text{H}}(w) \stackrel{\mathcal{N} \rightarrow \infty}{\cong} e^{-w}$ with $w \in [0, \infty)$ [42]. We are interested in states $|\Psi\rangle, |\Psi'\rangle$ of N q-qits generated by realisations $W(t_1), W'(t_2)$ of a quantum circuit of depths t_1, t_2 . Since when at least one between t_1 and t_2 is large, only the overall depth $t = t_1 + t_2$ is relevant (see Fig. 1(a)), we denote the overlap distribution by $p(w; N, t)$. However, our derivations also apply to the interesting case $t_2 = 0$, where a time-evolved state is decomposed in the computational bases, see below.

Ginibre ensemble and universality. — To begin, we consider a one-dimensional chain with $N = L$ q -dimensional sites. Although the argument applies in a more general form, it is useful to keep in mind a brick-wall RUC where each gate $u_{i,i+1}(t)$ acting on the sites $i, i+1$ at time t is chosen independently. We use the convention in which one even and odd layer are applied within a single time step $\Delta t = 1$. In this setting, the overlap w can be represented graphically as in Fig. 1(a). Upon averaging the ensemble, the calculation of w reduces to that of an appropriate partition function, summing up the states of each bond. It is useful to define a transfer matrix G_i in the spatial direction, which is the collection of all gates (and initial states) that act in the temporal direction on the i -th q-qits (red in Fig. 1(a)). We denote the product of such transfer matrices by

$$\mathcal{G} = G_1 G_2 \dots G_L. \quad (1)$$

Then, the overlap w can be expressed in terms of the matrix elements of \mathcal{G} : for periodic boundary conditions (pbc), one has $w = |\text{Tr}[\mathcal{G}]|^2$, while for open boundary conditions (obc), $w = |\ell^{\dagger} \mathcal{G} r|^2$ where ℓ, r are appropriate boundary vectors whose specific forms are not important. G_i are statistically uncorrelated matrices for different i -s, and are of size $M(t) \times M(t)$ with $M(t) = q^{4t-2}$ in the geometry of Fig. 1(a). Although the specific relation between $M(t)$ and t is model-dependent, the exponential growth is generic. In the following, we will omit time dependence of M unless needed. When both t and L are large, we end up with a product of a large number of large matrices, and this is a regime in which universality can emerge [40, 43–45]. In a coarse-grained picture, we group a number ℓ of these matrices $\tilde{G}_a := G_{a\ell+1} G_{a\ell+2} \dots G_{(a+1)\ell}$, with $\mathcal{G} = \prod_{a=1}^{L/\ell} \tilde{G}_a$, and for large enough ℓ , we can assume that there is no privileged basis so that rotational invariance emerges. Since the evolution in the spatial direction under generic many-body chaotic dynamic is non-Hermitian, the natural choice is to sample each \tilde{G}_a from the simplest non-Hermitian random matrices, the Ginibre ensemble, where all matrix elements of \tilde{G}_a are independently drawn complex Gaussian variables with zero average and variance ν^2 . In fact, the universality of the Ginibre ensemble has recently been shown to emerge from the dual transfer matrices associated to generic many-body quantum chaotic systems [43] and to non-hermitian dynamics due to quantum measurements [40]. To calculate the k -th moment

of w , we are interested in k copies of \mathcal{G} and \mathcal{G}^* , and from Wick's theorem we have the identity [40]

$$\mathbb{E}[\tilde{G}_a \otimes \tilde{G}_a^* \otimes \dots \otimes \tilde{G}_a \otimes \tilde{G}_a^*] = \nu^{2k} \sum_{\sigma \in S_k} |\sigma\rangle\langle\sigma|, \quad (2)$$

where $\mathbb{E}[\dots]$ denotes the ensemble average, and S_k is the symmetric group with k elements. To compactly account for Wick's contractions, we introduce the permutation states $|\sigma\rangle \in \mathbb{C}^{2Mk}$ according to $\langle\langle\alpha_1, \bar{\alpha}_1, \dots, \alpha_k, \bar{\alpha}_k|\sigma\rangle\rangle = \prod_{j=1}^k \delta_{\alpha_j, \bar{\alpha}_{\sigma_j}}$ and $\alpha, \bar{\alpha}$ are indices for rows (and columns) of \tilde{G}_a and \tilde{G}_a^* , respectively. Introducing the transfer matrix in the permutation space as $T_{\sigma, \sigma'} = \nu^{2k} \langle\langle\sigma|\sigma'\rangle\rangle = (\nu^2 M)^k M^{-d(\sigma, \sigma')}$ with $d(\sigma, \sigma')$ the transposition distance between permutations, we can write $\mathbb{E}[\mathcal{G}^{\otimes k}] = \sum_{\sigma, \sigma'} [T^{L/\ell-1}]_{\sigma, \sigma'} |\sigma\rangle\langle\sigma'|$. For large $M \gg 1$, we can expand $T(\sigma, \sigma') = (\nu^2 M)(\delta_{\sigma, \sigma'} + M^{-1} A_{\sigma, \sigma'} + O(M^{-2}))$, where $A_{\sigma, \sigma'}$ is the adjacency matrix of the transposition graph, i.e. it equals one if σ and σ' differ by one transposition, and vanishes otherwise. Introducing the Thouless length as $L_{\text{Th}}(t) \equiv M(t)\ell(t)$, we define the *Thouless scaling limit* where both L and t are large but such that $x \equiv L/L_{\text{Th}}(t)$ is kept constant [46]. In this limit, we obtain

$$\lim_{\substack{t, L \rightarrow \infty \\ x = L/L_{\text{Th}}(t)}} \mathbb{E}[w^k] = \sum_{\sigma, \sigma'} [e^{xA}]_{\sigma, \sigma'} \delta_{\sigma, \sigma'}^{(\text{bc})}, \quad (3)$$

where $\delta_{\sigma, \sigma'}^{(\text{bc})}$ reduces to Kronecker delta for pbc and to 1 for obc and we used the normalization $\mathbb{E}[w] = 1$ to fix $\nu^2 = M^{-1}$ [47]. The microscopic structure of the underlying circuit can only enter the scaling limit in setting the length scale $L_{\text{Th}}(t)$, while the general form of the moments only depends on the spectrum of the adjacency matrix A . Expanding in powers of x , one sees that Eq. (3) admits a simple interpretation as the grand canonical partition function of a dilute gas of domain walls, corresponding to transpositions connecting two permutations and each carrying a fugacity $\sim L_{\text{Th}}(t)^{-1}$ (Fig. 1(b)). Since a domain wall can be placed anywhere along the entire system, we obtain a factor $x = L/L_{\text{Th}}(t)$ for each of them. Finally, the composition of permutations and the boundary conditions impose selection rules on the allowed sequences of transpositions: e.g., at the n -th order, for periodic conditions, only closed paths of length n in the transposition graph are allowed, the number of which is given by $\text{tr}[A^n]$. In this perspective, the cost associated with an elementary transposition can be identified with the membrane cost associated with the purity for a depth t , i.e. $\Pi(t) \sim L_{\text{Th}}(t)^{-1}$ [48], thus justifying the exponential growth of $L_{\text{Th}}(t)$ on general grounds.

Random Phase Model (RPM). — To corroborate the universality derived in Eq. (3), let us now analyze the problem in the specific example of the RPM, introduced in [33]. We consider single-site Haar-random unitaries, $u_i^{(1)}(t)$, and two-site gates, $[u_{j, j+1}^{(2)}(t)]_{a_j a_{j+1}, a_j a_{j+1}} =$

$\exp[\varphi_{a_j, a_{j+1}}^{(j)}(t)]$, coupling neighbouring sites via a diagonal random phase ($a_j = 1, 2, \dots, q$). Each coefficient $\varphi_{a_j, a_{j+1}}^{(j)}(t)$ is an independent Gaussian random real variable with mean zero and variance ϵ , which controls the coupling strength between neighboring spins. Then, in the brick-wall geometry of Fig. 1(a), we choose gates on even/odd layers as $u_{j, j+1}(t) = u_{j, j+1}^{(2)}(t)u_j^{(1)}(t)u_{j+1}^{(1)}(t)$ or $u_{j, j+1}(t) = u_j^{(1)}(t)u_{j+1}^{(1)}(t)u_{j, j+1}^{(2)}(t)$ respectively, so that all commuting 2-site gates are applied one after the other. The model admits straightforward extensions to arbitrary $d > 1$ [27, 46]. Constraining the gates $u^{(j)}(t)$ and $\varphi^{(j)}(t)$ to be site- or time-independent (or both), this model gives access to translational invariant and Floquet models, as explored in [33, 43, 46, 49, 50]. Here we first consider the case where all gates are drawn independently in space and time postponing the discussion of the Floquet case to the end. Also, we consider the analytically tractable limit $q \rightarrow \infty$ at fixed coupling ϵ . In order to compute the moments of the overlap $\mathbb{E}[w^k]$, we consider k copies of the circuit and first consider the average over single-site random unitaries $u_j^{(1)}(t)$. Such an average can be once again expressed in terms of permutation states, using the formula $\mathbb{E}[u \otimes u^* \otimes \dots \otimes u \otimes u^*] = \sum_{\sigma, \tau \in S_k} \text{Wg}(\sigma\tau^{-1}) |\sigma\rangle\langle\tau| \stackrel{q \gg 1}{\approx} q^{-k} \sum_{\sigma \in S_k} |\sigma\rangle\langle\sigma|$, where $\text{Wg}(\sigma)$ denotes the Weingarten function [51]. Importantly, in contrast to Eq. (2), permutation states arise upon ensemble averaging at each group of unitaries located at each space-time coordinate, and the contraction between permutation states occurs in the temporal direction for each spatial site, i.e. the vertical direction along a fixed site in Fig. 1(a). The rapid decay of the overlap $\langle\langle\sigma|\sigma'\rangle\rangle = q^{k-d(\sigma, \sigma')}$ when $q \rightarrow \infty$ forces the permutations to be the same in time for every fixed j . In other words, the Haar average at large q leads to a sum over $k!^L$ possible permutations σ_j at each spatial site j . The choice of permutations between neighboring sites $j, j+1$ leads to different $\varphi^{(j)}$ random phase deletions. Specifically, the moments of the overlap can be expressed as

$$\mathbb{E}[w^k]_{\text{RPM}} = \sum_{\sigma_1, \dots, \sigma_L \in S_k} \prod_{j=1}^{L-1} [T_{\text{RPM}}]_{\sigma_j, \sigma_{j+1}} \delta_{\sigma_1, \sigma_L}^{(\text{bc})}. \quad (4)$$

where transfer matrix T_{RPM} is obtained by averaging over all phases between two neighbouring sites. Using that phases at different times are uncorrelated, we obtain $[T_{\text{RPM}}]_{\sigma, \sigma'} = \mathbb{E}[m_{\sigma, \sigma'}^{(k)}]^t$, where the coefficient $m_{\sigma, \sigma'}^{(k)}$ is the contribution from the random phase gate in $u_{j, j+1}^{(2)}(t)$ at a given a time slice, and takes the form

$$m_{\sigma, \sigma'}^{(k)} = q^{-2k} \sum_{\{a\}, \{b\}} \prod_{j=1}^k e^{i[\phi_{a_j, b_j} - \phi_{a_{\sigma(j)}, b_{\sigma'(j)}}]}, \quad (5)$$

where the summations runs over $a_i, b_i = 1, 2, \dots, q$, and contain repetitions when two or more indices a_i, b_i have

the same value. However, such coincidences can be ignored in the limit of large q , where we arrive at

$$\mathbb{E}[m_{\sigma,\sigma'}^{(k)}]_{\text{RPM}} = e^{-\epsilon[k-n_{\text{F}}(\sigma\sigma'^{-1})]}, \quad (6)$$

where $n_{\text{F}}(\sigma)$ counts the number of fixed points in permutation σ . With these expressions, we can now evaluate the moments in Eq. (4) and the frame potential $F_{\text{RPM}}^{(k)} = q^{-kL}\mathbb{E}[w^k]_{\text{RPM}}$. In the limit of large t at fixed L , the sum is dominated by the situation where all permutations are the same $\sigma_i = \sigma$ independently of i and one recovers the PT distribution. Additionally, setting in this case $L_{\text{Th}}(t) = e^{2\epsilon t}$, we can expand

$$[T_{\text{RPM}}]_{\sigma,\sigma'} = \delta_{\sigma,\sigma'} + \frac{A_{\sigma,\sigma'}}{L_{\text{Th}}(t)} + O(L_{\text{Th}}(t))^{-2} \quad (7)$$

where A is once again the adjacency matrix of transposition graph. Thus, introducing the scaling variable $x = L/L_{\text{Th}}(t)$, from Eq. (4) we recover Eq. (3).

Spectrum of adjacency matrix. — The matrix $A_{\sigma,\sigma'} = f(\sigma\sigma'^{-1})$ only depends on the difference between the elements σ,σ' in S_k . Also, $\forall \nu \in S_k, f(\nu\sigma\nu^{-1}) = f(\sigma)$, i.e. it depends only on the conjugacy class. We can see this as a generalization of a *circulant Toeplitz matrix* to a general group \mathbf{G} . In our case $\mathbf{G} = S_k$, while the standard case of circulant matrices corresponds to the cyclic group $\mathbf{G} = \mathbb{Z}_k$ [42]. Any such matrix can be diagonalised by a generalized Fourier transform, $A = U\Lambda U^\dagger$, where

$$U_{\sigma,(\rho,ij)} = \sqrt{\frac{\dim(\rho)}{k!}} R_\rho(\sigma^{-1})_{ij}, \quad (8)$$

where ρ labels the irreducible representations of S_k , $\dim(\rho)$ is the corresponding dimension and $R_\rho(\sigma)_{ij}$ are the components of the matrix representing the permutations σ on ρ . The matrix U is square and unitary as a consequence of the known identity $\sum_{\rho \in \text{Irr}(S_k)} \dim(\rho)^2 = k!$, where $\text{Irr}(S_k)$ are the irreducible representations of S_k . When applying Eq. (8), one has that the eigenvalues of A are independent of i,j and are thus in one-to-one correspondence with each irreps ρ of S_k , with a degeneracy $\dim(\rho)^2$. Their explicit form can be deduced from Eq. (8) and reads [47]

$$\nu(\rho) = \binom{k}{2} \frac{\chi_\rho(1^{k-2}2^1)}{\chi_\rho(1^k)} = \frac{1}{2} \sum_i [\rho_i^2 - (\rho_i^t)^2]. \quad (9)$$

where $\chi_\rho(\mu)$ denotes the character of the irreps ρ on the conjugacy class μ . In the second equality, we further simplified the expression using the identification between irreps of S_k and integer partitions of k . Thus, we denote $\rho = (\rho_1, \rho_2, \dots)$, with $\sum_i \rho_i = k$ and by ρ^t the dual partition, obtained exchanging rows and columns in the corresponding Young diagram, with $\rho_i^t = \#\{j | \rho_j \geq i\}$. Then, we can use Frobenius formula to express the characters and derive the last form [52].

We can now evaluate the scaling functions corresponding to the moments (3). Observe that $\rho = (k)$ corresponds to the trivial one-dimensional representation, $\forall \sigma \in S_k, R_{(k)}(\sigma) = 1$. It follows that for obc, we are simply evaluating e^{xA} on its maximal eigenvector, leading to

$$\mathbb{E}[w^k]_{\text{obc}} \stackrel{\text{obc}}{=} k! e^{x\nu(\rho=(k))} = k! e^{xk(k-1)/2}, \quad (10a)$$

$$\mathbb{E}[w^k]_{\text{pbc}} \stackrel{\text{pbc}}{=} \text{tr}[e^{xA}] = \sum_{\rho \vdash k} \dim(\rho)^2 e^{x\nu(\rho)}, \quad (10b)$$

where the last sum is over ρ integer partition of k .

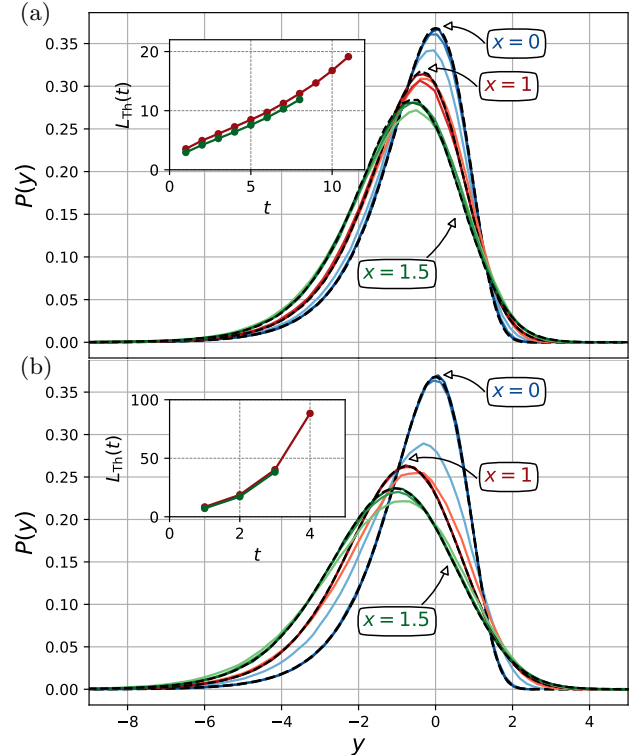


FIG. 2. Comparison of the distribution of $y = \log w$ between numerical simulation and the theoretical prediction (black dashed line) for different values of x and increasing value of the depth t , which is indicated with darker shades of the same color. For each t , the value of $L \sim L_{\text{Th}}(t)$ (shown in the insets) is chosen so that $\mathbb{E}[y]$ matches the theoretical prediction. (a): The pbc, numerical simulation of the RPM at $q = 2, \epsilon = 1$. For $x = 0$, we show the pairs $(t, L) \in \{(7, 8), (11, 8), (15, 8)\}$; for $x = 1$, $(t, L) \in \{(3, 6), (5, 9), (10, 17)\}$; for $x = 1.5$, $(t, L) \in \{(3, 8), (5, 11), (8, 18)\}$. The theoretical distribution of y was generated for $w = w_0 g$ using (12) and for a sample size $N_{\text{sample}} = 10^6$ at $n = 300$. (b): The obc, numerical simulation for a brick-wall model (BWM) where the local 2-site gate is chosen independently from the Haar distribution at $q = 2$. We show data for $x = 0$, $(t, L) \in \{(1, 6), (3, 6), (4, 6)\}$; for $x = 1$, $(t, L) \in \{(1, 8), (3, 40), (4, 88)\}$; for $x = 1.5$, $(t, L) \in \{(1, 11), (2, 26), (3, 57)\}$. The theoretical distribution $P(y)$ was created by the use of (11). Each numerical distributions were obtained from a sample size $N_{\text{sample}} = 1.5 \times 10^6$.

Probability distributions of the overlap. — Using

the information of the moments in Eq. (10), we can now extract the overlap distribution w . To do so, it is useful to write $w \stackrel{\text{in law}}{=} w_0 g$ as the product of two independent random variables, with w_0 distributed according to the PT $p_H(w_0)$, so that $\mathbb{E}[w_0^k] = k!$. The residual random variable g has a distribution that depends on the boundary conditions. For obc, one recognises that Eq. (10a) is obtained if g is drawn from the Lognormal($\mu = -x/2, \sigma^2 = x$). This implies the distribution in the scaling limit

$$p_{\text{obc}}(w; x) = \int \frac{du e^{-u^2/2+x}}{\sqrt{2\pi}} \exp\left[-we^{u\sqrt{x+\frac{3x}{2}}}\right]. \quad (11)$$

For pbc, the distribution of g leading to Eq. (10b) cannot be written down in simple terms. In [40], its generating function was expressed in terms of a determinant. Alternatively, in [42] (see also [53–55]) we show that

$$g_{\text{pbc}} \stackrel{\text{in law}}{=} \lim_{n \rightarrow \infty} \frac{1}{n} \text{tr} \left[e^{\sqrt{xn}H + xD} \right], \quad (12)$$

where H a standard $n \times n$ GUE random matrix with distribution $P(H) \propto \exp[-n\text{tr}[H^2]/2]$ and $D = \text{diag}(-1/2, -3/2, \dots, -(2n-1)/2)$. This form can be used to efficiently sample the distribution of $w = w_0 g$. In Fig. 2, we compare the theoretical prediction for both obc and pbc with numerical simulations of two different finite- q random circuits with excellent agreement.

Generalisation and discussion. — Firstly, an interesting extension are Floquet circuits [4, 33], where the same gates are repeated in time. In this case, a strong quenched spatial disorder can lead to many-body localization (MBL), where thermalization and scrambling are hindered [56–58]. However, at weak disorder, one can still be in a thermalising phase but where weak links play an important role affecting transport [59] and entanglement properties [60]. Following the arguments of [60], we expect the scenario in Fig. 1(b) to change because it is favorable to place domain walls in correspondence of weak links. However, after coarse graining, this only modifies the growth $\log L_{\text{Th}}(t) \propto t^\alpha$, where the exponent $\alpha < 1$ changes continuously with disorder strength. That the same distributions also apply to the Floquet case is confirmed by our simulations away from MBL [42].

Secondly, instead of considering the overlap between two different realizations of the circuit, we can consider the expansion of the state evolved by the circuit in the strings of the computational basis $w = |\langle \mathbf{a} = a_1, \dots, a_L | \Psi \rangle|^2$, which corresponds to taking $t_2 = 0$, $t = t_1$ and $L_{\text{Th}}(t = t_1)$. In this case, the distribution of w on the various string \mathbf{a} will still be described by the universal distributions we have identified here. This result is important because of its relevance in concrete experiments. For example, in [18, 61], the statistical distribution of the \mathbf{a} -strings of a state evolved from a random circuit was used in an attempt to demonstrate quantum supremacy: a measure of the fidelity of the ex-

periment was obtained precisely by assuming that w follows the PT distribution. However, here we showed that in the scaling regime the distribution is modified while remaining universal. For instance, the participation entropy [62–65] deviates for $x > 0$ from the PT one as $-\mathbb{E}[\log w]_{\text{obc}} = 1 - \gamma + x$, with γ the Euler’s constant.

Thirdly, large- q analysis applied to RPM, suggests that even for $d > 1$ the moment $\mathbb{E}[w^k]$ is described by mapping to a model in d -dimensions in which local degrees of freedom are permutations and the ferromagnetic Boltzmann weight $J(t)$ between sites grows exponentially with t . At large times, there exist $k!$ perfectly ordered groundstates. The excitations on top of these correspond to isolated defects [46], in which a site differs by a single transposition from its neighbors. Since a defect can be placed anywhere in volume $N = L^d$ and its presence breaks $2d$ ferromagnetic bonds, the scaling limit in this case corresponds to $x = N/N_{\text{th}}(t)$, with $N_{\text{th}}(t) = J(t)^{2d}$. There are $\binom{k}{2}$ choices of transpositions for each defect and summing over their number, we arrive at $\mathbb{E}[w^k]_{d>1} = k! \sum_{n=0}^{\infty} (k-1)/2^n x^n / n! = k! e^{k(k-1)x/2}$. This result coincides with Eq. (10a) and leads again to Eq. (11), although its origin is different in that at $d > 1$ the excitations are not domain walls but isolated defects. Numerical verification of this result is difficult, but recent quantum computing platforms offer a promising framework for observing our predictions including higher $d > 1$.

Acknowledgements. — ADL thanks Adam Nahum and Tianci Zhou for discussions. AChr acknowledges support from the EUTOPIA PhD Co-tutelle program. AChan acknowledges the support from the Royal Society grant RGS\R1\231444. ADL acknowledges support from the ANR JCJC grant ANR-21-CE47-0003 (TamEnt).

-
- [1] P. Calabrese, F. H. L. Essler, and G. Mussardo, Introduction to ‘quantum integrability in out of equilibrium systems’, *Journal of Statistical Mechanics: Theory and Experiment* **2016**, 064001 (2016).
 - [2] A. Nahum, J. Ruhman, S. Vijay, and J. Haah, Quantum entanglement growth under random unitary dynamics, *Phys. Rev. X* **7**, 031016 (2017).
 - [3] T. Rakovszky, F. Pollmann, and C. W. von Keyserlingk, Diffusive hydrodynamics of out-of-time-ordered correlators with charge conservation, *Phys. Rev. X* **8**, 031058 (2018).
 - [4] A. Chan, A. De Luca, and J. T. Chalker, Solution of a minimal model for many-body quantum chaos, *Phys. Rev. X* **8**, 041019 (2018).
 - [5] J. S. Cotler, G. Gur-Ari, M. Hanada, J. Polchinski, P. Saad, S. H. Shenker, D. Stanford, A. Streicher, and M. Tezuka, Black holes and random matrices, *Journal of High Energy Physics* **2017**, 10.1007/jhep05(2017)118 (2017).
 - [6] P. Hayden and J. Preskill, Black holes as mirrors: quantum information in random subsystems, *Journal of High Energy Physics* **2007**, 120 (2007).

- [7] D. DiVincenzo, D. Leung, and B. Terhal, Quantum data hiding, *IEEE Transactions on Information Theory* **48**, 580–598 (2002).
- [8] A. Ambainis and J. Emerson, Quantum t-designs: t-wise independence in the quantum world (2007), arXiv:quant-ph/0701126 [quant-ph].
- [9] D. Gross, K. Audenaert, and J. Eisert, Evenly distributed unitaries: On the structure of unitary designs, *Journal of Mathematical Physics* **48**, 10.1063/1.2716992 (2007).
- [10] D. A. Roberts and B. Yoshida, Chaos and complexity by design, *Journal of High Energy Physics* **2017**, 10.1007/jhep04(2017)121 (2017).
- [11] A. W. Harrow and R. A. Low, Random quantum circuits are approximate 2-designs, *Communications in Mathematical Physics* **291**, 257 (2009).
- [12] F. G. S. L. Brandão, A. W. Harrow, and M. Horodecki, Local random quantum circuits are approximate polynomial-designs, *Communications in Mathematical Physics* **346**, 397–434 (2016).
- [13] A. Chan and A. D. Luca, Projected state ensemble of a generic model of many-body quantum chaos (2024), arXiv:2402.16939 [quant-ph].
- [14] W. W. Ho and S. Choi, Exact emergent quantum state designs from quantum chaotic dynamics, *Phys. Rev. Lett.* **128**, 060601 (2022).
- [15] M. Ippoliti and W. W. Ho, Dynamical Purification and the Emergence of Quantum State Designs from the Projected Ensemble, *PRX Quantum* **4**, 030322 (2023), arXiv:2204.13657 [quant-ph].
- [16] M. Lucas, L. Piroli, J. De Nardis, and A. De Luca, Generalized deep thermalization for free fermions, *Phys. Rev. A* **107**, 032215 (2023).
- [17] S. Boixo, S. V. Isakov, V. N. Smelyanskiy, R. Babbush, N. Ding, Z. Jiang, M. J. Bremner, J. M. Martinis, and H. Neven, Characterizing quantum supremacy in near-term devices, *Nature Physics* **14**, 595 (2018).
- [18] F. Arute, K. Arya, R. Babbush, D. Bacon, J. C. Bardin, R. Barends, R. Biswas, S. Boixo, F. G. Brandao, D. A. Buell, *et al.*, Quantum supremacy using a programmable superconducting processor, *Nature* **574**, 505 (2019).
- [19] L. Susskind, Computational complexity and black hole horizons (2014), arXiv:1402.5674 [hep-th].
- [20] A. R. Brown and L. Susskind, Second law of quantum complexity, *Physical Review D* **97**, 10.1103/physrevd.97.086015 (2018).
- [21] J. Haferkamp, P. Faist, N. B. Kothakonda, J. Eisert, and N. Yunger Halpern, Linear growth of quantum circuit complexity, *Nature Physics* **18**, 528 (2022).
- [22] F. G. Brandão, W. Chemissany, N. Hunter-Jones, R. Kueng, and J. Preskill, Models of quantum complexity growth, *PRX Quantum* **2**, 030316 (2021).
- [23] Y. Sekino and L. Susskind, Fast scramblers, *Journal of High Energy Physics* **2008**, 065–065 (2008).
- [24] S. H. Shenker and D. Stanford, Black holes and the butterfly effect, *Journal of High Energy Physics* **2014**, 10.1007/jhep03(2014)067 (2014).
- [25] J. Maldacena, S. H. Shenker, and D. Stanford, A bound on chaos, *Journal of High Energy Physics* **2016**, 10.1007/jhep08(2016)106 (2016).
- [26] M. P. Fisher, V. Khemani, A. Nahum, and S. Vijay, Random quantum circuits, *Annual Review of Condensed Matter Physics* **14**, 335 (2023), <https://doi.org/10.1146/annurev-conmatphys-031720-030658>.
- [27] A. Nahum, S. Vijay, and J. Haah, Operator spreading in random unitary circuits, *Phys. Rev. X* **8**, 021014 (2018).
- [28] C. W. von Keyserlingk, T. Rakovszky, F. Pollmann, and S. L. Sondhi, Operator hydrodynamics, otocs, and entanglement growth in systems without conservation laws, *Phys. Rev. X* **8**, 021013 (2018).
- [29] V. Khemani, A. Vishwanath, and D. A. Huse, Operator spreading and the emergence of dissipation in unitary dynamics with conservation laws, *ArXiv e-prints* (2017), arXiv:1710.09835 [cond-mat.stat-mech].
- [30] A. Nahum, J. Ruhman, S. Vijay, and J. Haah, Quantum entanglement growth under random unitary dynamics, *Phys. Rev. X* **7**, 031016 (2017).
- [31] A. Nahum, J. Ruhman, and D. A. Huse, Dynamics of entanglement and transport in one-dimensional systems with quenched randomness, *Phys. Rev. B* **98**, 035118 (2018).
- [32] T. Zhou and A. Nahum, Emergent statistical mechanics of entanglement in random unitary circuits, *Phys. Rev. B* **99**, 174205 (2019).
- [33] A. Chan, A. De Luca, and J. T. Chalker, Spectral statistics in spatially extended chaotic quantum many-body systems, *Phys. Rev. Lett.* **121**, 060601 (2018).
- [34] A. J. Friedman, A. Chan, A. De Luca, and J. T. Chalker, Spectral statistics and many-body quantum chaos with conserved charge, *Phys. Rev. Lett.* **123**, 210603 (2019).
- [35] P. Kos, M. Ljubotina, and T. Prosen, Many-body quantum chaos: Analytic connection to random matrix theory, *Physical Review X* **8**, 10.1103/physrevx.8.021062 (2018).
- [36] B. Bertini, P. Kos, and T. Prosen, Exact Spectral Form Factor in a Minimal Model of Many-Body Quantum Chaos, *Phys. Rev. Lett.* **121**, 264101 (2018), arXiv:1805.00931.
- [37] S. Mullane, Sampling random quantum circuits: a pedestrian’s guide (2020), arXiv:2007.07872 [quant-ph].
- [38] N. Hunter-Jones, Unitary designs from statistical mechanics in random quantum circuits (2019).
- [39] T. Zhou and A. Nahum, Entanglement membrane in chaotic many-body systems, *Phys. Rev. X* **10**, 031066 (2020).
- [40] A. De Luca, C. Liu, A. Nahum, and T. Zhou, Universality classes for purification in nonunitary quantum processes (2023), arXiv:2312.17744 [cond-mat.stat-mech].
- [41] M. L. Mehta, *Random Matrices* (Academic Press, 2004).
- [42] See supplemental material for additional details.
- [43] S. Shivam, A. De Luca, D. A. Huse, and A. Chan, Many-body quantum chaos and emergence of ginibre ensemble, *Physical Review Letters* **130**, 10.1103/physrevlett.130.140403 (2023).
- [44] D.-Z. Liu, D. Wang, and Y. Wang, Lyapunov exponent, universality and phase transition for products of random matrices (2022), arXiv:1810.00433 [math.PR].
- [45] G. Akemann, Z. Burda, and M. Kieburg, Universality of local spectral statistics of products of random matrices, *Phys. Rev. E* **102**, 052134 (2020).
- [46] A. Chan, S. Shivam, D. A. Huse, and A. De Luca, Many-body quantum chaos and space-time translational invariance, *Nature Communications* **13**, 10.1038/s41467-022-34318-1 (2022).
- [47] For obc, we could get rid of the boundary states using that $\sum_{\alpha, \bar{\alpha}} \ell_{\alpha_1} \ell_{\bar{\alpha}_1}^* \dots \ell_{\alpha_k} \ell_{\bar{\alpha}_k}^* \langle \alpha_1, \bar{\alpha}_1, \dots, \alpha_k, \bar{\alpha}_k | \sigma \rangle = |\ell|^{2k}$, which we can absorb in the definition of ν .

- [48] C. Jonay, D. A. Huse, and A. Nahum, Coarse-grained dynamics of operator and state entanglement (2018), arXiv:1803.00089 [cond-mat.stat-mech].
- [49] A. Chan, A. De Luca, and J. T. Chalker, Spectral Lyapunov exponents in chaotic and localized many-body quantum systems, *Phys. Rev. Research* **3**, 023118 (2021).
- [50] K. Huang, X. Li, D. A. Huse, and A. Chan, Out-of-time-order correlator, many-body quantum chaos, light-like generators, and singular values (2023), arXiv:2308.16179 [quant-ph].
- [51] D. Weingarten, Asymptotic behavior of group integrals in the limit of infinite rank, *Journal of Mathematical Physics* **19**, 999 (1978), <https://doi.org/10.1063/1.523807>.
- [52] S. R. E. Ingram, Some characters of the symmetric group, *Proceedings of the American Mathematical Society* **1**, 358 (1950).
- [53] F. Gerbino, P. L. Doussal, G. Giachetti, and A. De Luca, A dyson brownian motion model for weak measurements in chaotic quantum systems (2024), arXiv:2401.00822 [cond-mat.stat-mech].
- [54] T. Claeys and D. Wang, Random matrices with equispaced external source, *Communications in Mathematical Physics* **328**, 1023 (2014).
- [55] E. Brézin and S. Hikami, Level spacing of random matrices in an external source, *Phys. Rev. E* **58**, 7176 (1998).
- [56] R. Nandkishore and D. A. Huse, Many-body localization and thermalization in quantum statistical mechanics, *Annual Review of Condensed Matter Physics* **6**, 15 (2015), <https://doi.org/10.1146/annurev-conmatphys-031214-014726>.
- [57] F. Alet and N. Laflorencie, Many-body localization: An introduction and selected topics, *Comptes Rendus Physique* **19**, 498 (2018), quantum simulation / Simulation quantique.
- [58] D. A. Abanin and Z. Papić, Recent progress in many-body localization, *Annalen der Physik* **529**, 1700169 (2017), 1700169.
- [59] D. J. Luitz and Y. B. Lev, The ergodic side of the many-body localization transition, *Annalen der Physik* **529**, 1600350 (2017).
- [60] A. Nahum, J. Ruhman, and D. A. Huse, Dynamics of entanglement and transport in 1d systems with quenched randomness (2017), arXiv:1705.10364 [cond-mat.dis-nn].
- [61] S. Boixo, S. V. Isakov, V. N. Smelyanskiy, R. Babbush, N. Ding, Z. Jiang, M. J. Bremner, J. M. Martinis, and H. Neven, Characterizing quantum supremacy in near-term devices, *Nature Physics* **14**, 595–600 (2018).
- [62] N. Macé, F. Alet, and N. Laflorencie, Multifractal scalings across the many-body localization transition, *Phys. Rev. Lett.* **123**, 180601 (2019).
- [63] A. Bäcker, M. Haque, and I. M. Khaymovich, Multifractal dimensions for random matrices, chaotic quantum maps, and many-body systems, *Physical Review E* **100**, 10.1103/physreve.100.032117 (2019).
- [64] X. Turkeshi, M. Schirò, and P. Sierant, Measuring non-stabilizerness via multifractal flatness, *Physical Review A* **108**, 10.1103/physreva.108.042408 (2023).
- [65] X. Turkeshi and P. Sierant, (2024), arXiv:to appear [cond-mat.stat-mech].
- [66] R. M. Gray, Toeplitz and circulant matrices: A review, *Foundations and Trends® in Communications and Information Theory* **2**, 155 (2006).
- [67] P. Diaconis, *Group Representations in Probability and Statistics* (IMS, 1988).
- [68] I. G. Macdonald, *Symmetric functions and Hall polynomials* (Oxford university press, 1998).
- [69] P. J. Forrester, Meet andréief, bordeaux 1886, and andreev, kharkov 1882–1883, *Random Matrices: Theory and Applications* **08**, 1930001 (2019).
- [70] B. Jonnadula, J. P. Keating, and F. Mezzadri, Symmetric function theory and unitary invariant ensembles, *Journal of Mathematical Physics* **62**, 093512 (2021).
- [71] N. Macé, Quantum circuit at criticality (2019), arXiv:1912.09489 [cond-mat.dis-nn].

Supplementary Material

Universal distributions of overlaps from unitary dynamics in generic quantum many-body systems

In this supplementary material we provide additional details about:

- A. Haar ensemble
- B. Models
- C. Diagonalisation of the transfer matrix
- D. Numerical simulations

Appendix A: Haar ensemble

The Haar state ensemble is defined as $\mathcal{E}_H := \{U |\Psi_0\rangle \mid U \sim \text{Haar}[U(\mathcal{N})]\}$. To evaluate observables relating to the Haar ensemble, we recall the formula for the ensemble average of the moments of a Haar-random unitary matrix U ,

$$\mathbb{E} [U_{i_1 j_1} \cdots U_{i_n j_n} U_{k_1 l_1}^* \cdots U_{k_m l_m}^*] = \delta_{n,m} \sum_{\sigma, \tau \in S_n} \text{Wg}(\sigma\tau^{-1}) \prod_{\mu=1}^n \delta_{i_\mu, k_{\sigma(\mu)}} \delta_{j_\mu, l_{\tau(\mu)}}, \quad (\text{SA.1})$$

where $\text{Wg}(\sigma)$ is the Weingarten function [51]. S_n is the permutation group of n objects. $\delta_{i,j}$ is the Kronecker delta function. The Weingarten function $\text{Wg}(\sigma)$ simplifies as the dimension of the Haar-random unitaries, \mathcal{N} , increase:

$$\text{Wg}(\sigma) \stackrel{\mathcal{N} \rightarrow \infty}{\cong} \prod_i \mathcal{N}^{1-|\mathcal{C}_i(\sigma)|} (-1)^{|\mathcal{C}_i(\sigma)|-1} c_{|\mathcal{C}_i(\sigma)|-1}, \quad (\text{SA.2})$$

where \mathcal{C}_i is the i -th cycle in the cycle-decomposition of σ , and $|\mathcal{C}|$ is the size of the cycle \mathcal{C} , i.e. the number of elements it contains. $c_m = (2m)!/m!(m+1)!$ is the Catalan number.

The k -th moment of the density matrix can now be evaluated as,

$$\rho_{\text{Haar}}^{(k)} \equiv \rho^{(k)}[\mathcal{E}_{\text{Haar}}] = \sum_{\sigma, \tau \in S_k} \text{Wg}(\sigma\tau^{-1}) \text{Tr}[\tau (|\Psi\rangle \langle \Psi|)^{\otimes k}] \sigma \quad (\text{SA.3})$$

$$= \sum_{\tau \in S_k} \text{Wg}(\tau) \sum_{\sigma \in S_k} \sigma = \frac{\sum_{\sigma \in S_k} \sigma_k}{\mathcal{N}(\mathcal{N}+1) \cdots (\mathcal{N}+k-1)}, \quad (\text{SA.4})$$

where σ acts on the k -replicated space. In the third equality, we have used the fact that $\text{Tr}[\tau (|\Psi\rangle \langle \Psi|)^{\otimes k}] = 1$ due to normalization of the density matrix. In the last equality, we evaluated the summation of Weingarten functions $\text{Wg}(\sigma)$ over all permutations $\sigma \in S_n$, which can be obtained by considering the normalization condition,

$$1 = \text{Tr}[\rho_{\text{Haar}}^{(k)}] = \sum_{\tau} \text{Wg}(\tau) \sum_{\sigma} \text{Tr}[\sigma] = \sum_{\tau} \text{Wg}(\tau) \sum_{\sigma} \mathcal{N}^{r(\sigma)} = \sum_{\tau} \text{Wg}(\tau) \mathcal{N}(\mathcal{N}+1) \cdots (\mathcal{N}+k-1), \quad (\text{SA.5})$$

where $r(\sigma)$ denotes the number of cycle in permutation σ , and in the last equality we used standard combinatorial arguments to count the total number of cycles in permutations. Similarly, the frame potential can be evaluated as,

$$F_{\text{Haar}}^{(k)} \equiv F^{(k)}[\mathcal{E}_{\text{Haar}}] = \frac{k!}{\mathcal{N}(\mathcal{N}+1) \cdots (\mathcal{N}+k-1)} \stackrel{\mathcal{N} \rightarrow \infty}{\cong} \frac{k!}{\mathcal{N}^k}. \quad (\text{SA.6})$$

Appendix B: Models

In this work, we focus on the quantum circuits with the brick-wall geometry as models of quantum many-body systems. Such models are defined with an evolution operator given by

$$W(t) = \prod_{s=1}^t \tilde{W}(s), \quad \tilde{W}(s) = \bigotimes_{j \in 2\mathbb{Z}+s \bmod 2} u_{j,j+1}(s). \quad (\text{SB.1})$$

For spatial-temporal random circuits, the two-site gates $u_{j,j+1}(s)$ are independent random variables drawn from the same ensemble for different i and s . For Floquet model, $u_{j,j+1}$ are identical for different s .

We consider 2 generic many-body quantum chaotic models below. For the *brick-wall model* (BWM) [27], $u_{i,i+1}(s)$ are independent random matrices drawn according to

$$u_{j,j+1}^{\text{BWM}}(s) \in \text{CUE}(q^2), \quad (\text{SB.2})$$

where $\text{CUE}(n)$ is the circular unitary ensemble of unitaries of size n . For completeness, we repeat the definition of the random phase model here. For the *random phase model* (RPM) [33], we consider single-site Haar-random unitaries, $u_i^{(1)}(t)$, and two-site gates, $[u_{j,j+1}^{(2)}(t)]_{a_j a_{j+1}, a_j a_{j+1}} = \exp[\varphi_{a_j, a_{j+1}}^{(j)}(t)]$, coupling neighbouring sites via a diagonal random phase ($a_j = 1, 2 \dots, q$). Each coefficient $\varphi_{a_j, a_{j+1}}^{(j)}(t)$ is an independent Gaussian random real variable with mean zero and variance ϵ , which controls the coupling strength between neighboring spins. Then, in the brick-wall geometry, $u_{i,i+1}(s)$ are independent random matrices drawn according to

$$u_{j,j+1}^{\text{RPM}}(s) = \begin{cases} u_{j,j+1}^{(2)}(s) u_j^{(1)}(s) u_{j+1}^{(1)}(s), & j \text{ even}, \\ u_j^{(1)}(t) u_{j+1}^{(1)}(t) u_{j,j+1}^{(2)}(t), & j \text{ odd}, \end{cases} \quad (\text{SB.3})$$

so that all commuting 2-site gates are applied one after the other.

Appendix C: Diagonalisation of the transfer matrix

An n -by- n matrix M is a Toeplitz matrix [66] if $M_{ij} = m(i-j)$ with $i, j = 1, 2, \dots, n$ for some function m . As explained in the main text, given any function $f : \mathcal{G} \rightarrow \mathbb{C}$, we can generalise the notion of the Toeplitz matrix to an arbitrary group \mathcal{G} introducing a $|\mathcal{G}| \times |\mathcal{G}|$ matrix (with $|\mathcal{G}|$ the order of the group \mathcal{G}):

$$F_{\sigma, \sigma'} = f(\sigma \sigma'^{-1}), \quad \forall \sigma, \sigma' \in \mathcal{G}. \quad (\text{SC.1})$$

Similarly to the case of standard Toeplitz matrices, the spectrum can be investigated using a generalized notion of the Fourier transform [66]. Given a finite group \mathcal{G} , the group's representations $\rho : G \rightarrow \text{GL}(d_\rho, \mathbb{C})$ with dimension d_ρ , and a function $f : \mathcal{G} \rightarrow \mathbb{C}$, we define its Fourier transform $\hat{f}(\rho)$ as a function over the space of representations of \mathcal{G} which reads

$$\hat{f}(\rho) = \sum_{\sigma \in \mathcal{G}} f(\sigma) \rho(\sigma). \quad (\text{SC.2})$$

The inverse of this relation can be shown to be given by [67]

$$f(g) = \frac{1}{|\mathcal{G}|} \sum_{\rho \in \text{Irr}(\mathcal{G})} \dim(\rho) \text{Tr}[\rho(g^{-1}) \hat{f}(\rho)], \quad (\text{SC.3})$$

where the sum is restricted to the irreducible representation $\text{Irr}(\mathcal{G})$. The nice property of this Fourier transform is that it converts convolutions into product. In other words for two functions $h, g : \mathcal{G} \rightarrow \mathbb{C}$, one gets

$$h(\sigma) = \sum_{\sigma' \in \mathcal{G}} f(\sigma \sigma'^{-1}) g(\sigma') \quad \Rightarrow \quad \hat{h}(\rho) = \hat{f}(\rho) \hat{g}(\rho). \quad (\text{SC.4})$$

Now let's consider an eigenvector of the matrix F in Eq. (SC.1). Labelling its components as $c(\sigma)$ for any $\sigma \in \mathcal{G}$, it must satisfy

$$\sum_{\sigma' \in \mathcal{G}} f(\sigma \sigma'^{-1}) c(\sigma') = \lambda c(\sigma). \quad (\text{SC.5})$$

Taking the Fourier transform of both side, this implies

$$\hat{f}(\rho) \hat{c}(\rho) = \lambda \hat{c}(\rho), \quad \forall \rho \in \text{Irr}(\mathcal{G}) \quad (\text{SC.6})$$

Note that each side of this equation are matrices of size $\dim(\rho) \times \dim(\rho)$. To solve this equation, let's write the spectral decomposition of the matrix $\hat{f}(\rho)$ in bracket notation:

$$\hat{f}(\rho) = \sum_{j=1}^{\dim(\rho)} \lambda_j(\rho) |j\rangle \langle j|. \quad (\text{SC.7})$$

Then, we see that for any $\tilde{\rho} \in \text{Irr}(\mathcal{G})$ and any pair $i, j \in \{1, \dots, \dim(\rho)\}$, the following choice of $\hat{c}(\rho)$ provides a solution of Eq. (SC.6)

$$\hat{c}(\rho) \equiv \hat{c}^{(i,j,\tilde{\rho})}(\rho) = \begin{cases} 0, & \rho \neq \tilde{\rho}, \\ |i\rangle \langle j|, & \rho = \tilde{\rho}, \end{cases} \quad (\text{SC.8})$$

where $|i\rangle$ and $\langle j|$ refer respectively to the right and left eigenvectors of $\hat{f}(\rho)$. Once plugged in Eq. (SC.6), it leads to

$$\hat{f}(\rho) \hat{c}^{(i,j,\tilde{\rho})}(\rho) = \lambda_i(\tilde{\rho}) \hat{c}^{(i,j,\tilde{\rho})}(\rho). \quad (\text{SC.9})$$

This shows that the spectrum of the matrix F is given by the $\lambda_i(\rho)$ for $\rho \in \text{Irr}(\mathcal{G})$ and $i = 1, \dots, \dim(\rho)$ with a degeneracy $\dim(\rho)$, labeled by the index j . This provides a full spectral decomposition, since one has the known equality

$$\sum_{\rho \in \text{Irr}(\mathcal{G})} \dim(\rho)^2 = |\mathcal{G}|. \quad (\text{SC.10})$$

Now let us consider the case where the function f is a class function, i.e. it is invariant under the group conjugation

$$f(\omega\sigma\omega^{-1}) = f(\sigma), \quad (\text{SC.11})$$

for every $\omega, \sigma \in \mathcal{G}$. In this case, one can see that

$$[\hat{f}(\rho), \rho(\sigma)] = 0, \quad \forall \sigma \in \mathcal{G}. \quad (\text{SC.12})$$

Indeed, by definition we have

$$\begin{aligned} \hat{f}(\rho)\rho(\sigma) &= \sum_{\sigma' \in \mathcal{G}} f(\sigma') \rho(\sigma') \rho(\sigma) = \sum_{\sigma' \in \mathcal{G}} f(\sigma') \rho(\sigma' \sigma) = \sum_{\sigma'' \in \mathcal{G}} f(\sigma'' \sigma^{-1}) \rho(\sigma'') = \\ &= \sum_{\sigma'' \in \mathcal{G}} f(\sigma^{-1} \sigma'') \rho(\sigma'') = \sum_{\sigma''' \in \mathcal{G}} f(\sigma''') \rho(\sigma \sigma''') = \rho(\sigma) \sum_{\sigma''' \in \mathcal{G}} f(\sigma''') \rho(\sigma''') = \rho(\sigma) \hat{f}(\rho). \end{aligned} \quad (\text{SC.13})$$

Because of Schur's lemma, if $\rho \in \text{Irr}(\mathcal{G})$, $\hat{f}(\rho)$ must be a multiple of the identity

$$\hat{f}(\rho) = \lambda(\rho) \mathbb{1}, \quad (\text{SC.14})$$

and therefore in the spectral decomposition Eq. (SC.7), $\lambda_j(\rho) = \lambda(\rho)$ for all j 's. For generalised Toeplitz matrices obtained by class functions, the eigenvalues are labelled by the irreducible representations ρ and each has a degeneracy given by $\dim(\rho)^2$. We can finally obtain an equation for $\lambda(\rho)$ by taking the trace of both sides in Eq. (SC.2) and using (SC.14)

$$\text{Tr}[\hat{f}(\rho)] = \dim(\rho) \lambda(\rho) = \sum_{\sigma \in \mathcal{G}} f(\sigma) \chi_\rho(\sigma), \quad (\text{SC.15})$$

where $\chi_\rho(\sigma) = \text{Tr}[\rho(\sigma)]$ is the character of the representation ρ . Since both the function f and the character are class function, we can rewrite the sum as a sum over conjugacy classes $\text{Cl}(\mathcal{G})$

$$\lambda(\rho) = \sum_{\sigma \in \mathcal{G}} \frac{f(\sigma) \chi_\rho(\sigma)}{\chi_\rho(1)} = \sum_{\mu \in \text{Cl}(\mathcal{G})} \frac{f(\mu) \chi_\rho(\mu) \dim(\mu)}{\chi_\rho(1)}, \quad (\text{SC.16})$$

where we used that $\chi_\rho(1) = \dim(\rho)$, since the representation of the neutral element is the $\dim(\rho)$ dimensional identity and we denote as $\dim(\mu)$ the size of the conjugacy class μ . As a consistency check, we can look at the trivial case where $f(\mu) = 1$ irrespectively of μ . In this case, from Eq. (SC.16), we have

$$\lambda(\rho) = \sum_{\sigma \in \mathcal{G}} \frac{\chi_\rho(\sigma)}{\chi_\rho(1)} = \delta_{\rho,1} |\mathcal{G}|, \quad (\text{SC.17})$$

where we indicate as $\rho = 1$ the trivial one-dimensional representation where all elements are sent to 1. Eq. (SC.17) from the orthogonality of the characters

$$\frac{1}{|\mathcal{G}|} \sum_{\sigma \in \mathcal{G}} \chi_\rho(\sigma) \chi_{\rho'}(\sigma) = \delta_{\rho,\rho'}, \quad (\text{SC.18})$$

choosing $\rho' = 1$. Eq. (SC.17) is consistent with the fact that for $f = 1$, the matrix F reduces to a matrix made of 1's, which thus has only one non-vanishing eigenvalue and which equals the size of the matrix itself, i.e. $|\mathcal{G}|$.

Appendix D: Derivation of Eq. (12) in the main text

We start using the standard results of [55] about the spectrum of a random matrix with an external deterministic source. Consider a matrix M distributed according to

$$\text{Pro}(M) = \exp[-n \text{Tr}[V(M) - AM]], \quad (\text{SD.1})$$

where V is the potential and A is a deterministic matrix that we can assume to be diagonal without loss of generality $A = \text{diag}(a_1, \dots, a_n)$. Then, the eigenvalues $\{w_1, \dots, w_n\}$ of M follow the joint probability distribution

$$\text{Pro}(w_1, \dots, w_n) = \frac{1}{Z_n} \det(w_\alpha^{k-1})_{\alpha,k=1}^n \det(e^{n a_k w_\alpha})_{\alpha,k=1}^n \prod_{\alpha=1}^n e^{-n V(w_\alpha)}, \quad (\text{SD.2})$$

where the constant Z_n enforces normalisation. For Eq. (12), one sets

$$M = \sqrt{xn} H + xD, \quad (\text{SD.3})$$

where H and D are as defined in the main text, which is equivalent to choosing in Eq. (SD.2)

$$V(M) = \frac{M^2}{2xn}, \quad A = \frac{D}{n}, \quad (\text{SD.4})$$

leading to

$$\text{Pro}(w_1, \dots, w_n) = \frac{1}{Z_n} \det(w_\alpha^{k-1})_{\alpha,k=1}^n \det(e^{-(k-1/2)w_\alpha})_{\alpha,k=1}^n e^{-\sum_{\alpha=1}^n \frac{w_\alpha^2}{2x}}. \quad (\text{SD.5})$$

We are interested in computing the moments of $\text{Tr}[e^M]$, i.e.

$$\Omega_k(x) := \left\langle \left(\sum_{\alpha} e^{w_\alpha} \right)^k \right\rangle = \int dw_1 \dots dw_n \text{Pro}(w_1, \dots, w_n) \left(\sum_{\alpha} e^{w_\alpha} \right)^k. \quad (\text{SD.6})$$

The calculation will be analogous to [53], but we report it here with the appropriate notation and normalisations for convenience. As a proxy for the calculation of $\Omega_k(x)$, we first introduce Schur's polynomials. To an integer partition $\rho = (\rho_1, \dots, \rho_n)$ of the integer $k = \sum_{j=1}^n \rho_j$, with $\rho_1 \geq \rho_2 \geq \dots \geq \rho_n \geq 0$, one associates the corresponding Schur polynomial in n variables y_1, \dots, y_n via [68]

$$s_\rho(y) := \frac{\det(y_\alpha^{\rho_j + n - j})_{j,\alpha=1}^n}{\det(y_\alpha^{k-1})_{k,\alpha=1}^n} = \frac{\det(y_\alpha^{h_j})_{j,\alpha=1}^n}{\det(y_\alpha^{k-1})_{k,\alpha=1}^n}, \quad (\text{SD.7})$$

where we denote $h_j \equiv \rho_j + n - j$. Schur polynomials are symmetric and homogeneous of degree k . Setting $y_\alpha = e^{w_\alpha}$ and using the Vandermonde determinant formula

$$\det(y_\alpha^{k-1})_{\alpha,k=1}^n = \prod_{\alpha < \beta} (y_\beta - y_\alpha), \quad (\text{SD.8})$$

we can deduce

$$(-1)^{n(n-1)/2} e^{(n-1/2)\sum_\alpha w_\alpha} \det(e^{-(k-1/2)w_\alpha})_{\alpha,k=1}^n = \det(e^{(k-1)w_\alpha})_{\alpha,k=1}^n, \quad (\text{SD.9})$$

which allows us to express the average as

$$\langle s_\rho(y = e^w) \rangle = \frac{(-1)^{n(n-1)/2}}{Z_n} \int dw_1 \dots dw_n \det(w_\alpha^{k-1})_{\alpha,k=1}^n \det(e^{w_\alpha(h_j - n + 1/2)})_{j,\alpha=1}^n e^{-\sum_{\alpha=1}^n \frac{w_\alpha^2}{2x}}. \quad (\text{SD.10})$$

We can use Andreief identity [69] to express it in terms of a single determinant

$$\langle s_\rho(y) \rangle = \frac{(-1)^{n(n-1)/2} (2\pi x)^{n/2} n!}{Z_n} \det(I_{k,\rho_j - j + 1/2})_{k,j=1}^n, \quad (\text{SD.11})$$

where we defined

$$I_{k,\ell} = \int_{-\infty}^{\infty} \frac{dw}{\sqrt{2\pi x}} w^{k-1} e^{\ell w - \frac{w^2}{2x}} = \partial_\mu^{k-1} \left[e^{x\mu^2/2} \right] \Big|_{\mu=\ell} = \left(-i\sqrt{\frac{x}{2}} \right)^{k-1} e^{\ell^2 x/2} H_{k-1} \left(i\ell\sqrt{x/2} \right), \quad (\text{SD.12})$$

and in the last equality we used the Hermite polynomials $H_p(z) = (-1)^p e^{z^2} \partial_z^p [e^{-z^2}]$. Note that in these conventions, the leading coefficient is $H_p(z) = 2^p z^p + O(z^{p-1})$. Thus, by using the properties of determinants, we can combine the rows to extract only the leading coefficient out of each Hermite polynomials, obtaining

$$\det[I_{k,\rho_j - j + 1/2}]_{k,j=1}^n = x^{n(n-1)/2} \exp \left[\frac{x}{2} \sum_j (\rho_j - j + 1/2)^2 \right] \det[(\rho_j - j + 1/2)^{k-1}]. \quad (\text{SD.13})$$

This last determinant is once again a Vandermonde one which can be expressed via (SD.8). We can now plug this back in Eq. (SD.11) and fix the normalization Z_n using that for the trivial partition of 0, $\rho_1 = \rho_2 = \dots \rho_n = 0$, so that $s_{\rho=0}(y) = 1$ identically. We finally obtain

$$\langle s_\rho(y) \rangle = \exp \left[\frac{x}{2} \sum_j (\rho_j - j + 1/2)^2 - (j + 1/2)^2 \right] s_\rho(1), \quad (\text{SD.14})$$

where we recognized the equality

$$\prod_{1 \leq j < j' \leq n} \frac{\rho_j - \rho_{j'} - j + j'}{j' - j} = s_\rho(y_1 = 1, \dots, y_n = 1), \quad (\text{SD.15})$$

which expresses the number of semistandard Young diagram of shape ρ and n entries [68]. Eq. (SD.14) is consistent with the fact that for $x = 0$, the distribution (SD.5) reduces to $\text{Pro}(w_1, \dots, w_n) = \prod_\alpha \delta(w_\alpha)$ as the matrix M vanishes identically. Then, using the identity [68]

$$\sum_j (j-1)\rho_j = \frac{1}{2} \sum_i \rho_j^t (\rho_j^t - 1), \quad (\text{SD.16})$$

with ρ^t the dual partition of ρ , we obtain that

$$\frac{1}{2} \sum_j (\rho_j - j + 1/2)^2 - (j + 1/2)^2 = \nu(\rho), \quad (\text{SD.17})$$

as defined in Eq. (9). Now, we can relate the average of Schur polynomials to $M_k(x)$ using (see Eq. 3.10 in [70])

$$\left(\sum_\alpha y_\alpha \right)^k = \sum_{\rho^t = k} \dim(\rho) s_\rho(y) \quad \Rightarrow \quad M_k(x) = \sum_{\rho^t = k} \dim(\rho) e^{x\nu(\rho)} s_\rho(1). \quad (\text{SD.18})$$

Finally, we consider the limit of large n . We have the standard identity [68]

$$\lim_{n \rightarrow \infty} \frac{s_\rho(1)}{n^k} = \frac{\dim(\rho)}{k!}, \quad (\text{SD.19})$$

which leads to the final result employed in the main text

$$\mathbb{E}(g^k) = \lim_{n \rightarrow \infty} \frac{M_k(x)}{n^k} = \frac{1}{k!} \sum_{\rho^{\vdash k}} \dim(\rho)^2 e^{x\nu(\rho)}. \quad (\text{SD.20})$$

Appendix E: Numerical simulations

In this section we provide additional numerical results on the temporal-random and Floquet variations of two models, RPM and BWM, defined in Appendix B.

1. Temporal-random circuits

In the main text, we have demonstrated the convergence of the RPM, BWM in the pbc and obc cases. In this section, we further validate our findings by showcasing their consistency with the theoretical prediction in the complementary boundary conditions as demonstrated in Fig. S1. Fig. S2 serves to explicitly confirm the universality of the Thouless scaling limit as predicted by our theoretical framework. The numerical results in this paper were obtained in the following way:

- *RPM*: The simulation was carried out in the time direction for systems up to maximum size $L_{\max} = 20$ and up to maximum time $t_{\max} = 20$ with an effective coupling strength $\epsilon = 1$ and $q = 2$. We computed the states of $|\Psi(t)\rangle = W(t)|\Psi_0\rangle$, which in turn were used to generate the ensemble of $w = \mathcal{N}|\langle\Psi|\Psi'\rangle|^2$ for a sample size of $N_{\text{sample}} = 1.5 \times 10^6$.
- *BWM*: Similarly, we obtained the ensemble w using the same methodology as for the RPM with $q = 2$, $L_{\max} = 20$, $t_{\max} = 20$, but with employing the unitary circular ensemble (CUE) for the local gate $u_{j,j+1}(t)$. The BWM poses a greater numerical challenge due to the rapid growth of $L_{\text{Th}}(t)$ over time, as observed in Fig. S1 and Fig. 2. To address this, we employed the spatial transfer matrix method for simulating $\langle\Psi|\Psi'\rangle$ with $L_{\max} = 120$ and $t_{\max} = 5$. This method was specifically applied for the obc case, as the pbc scenario necessitates even more demanding computations, where we reached up to $t_{\max} = 2$.

The theoretical distributions of the random variable $y = \log w$ were found using (11),(12) for obc and pbc, respectively. This analysis was carried out for $N_{\text{sample}} = 10^6$ at $x = 0, 0.5, 1, 1.5$. Fig. S3, illustrates that in the obc scenario, the distribution exhibits robust n -convergence at $n = 300$, which was utilized for numerical comparison. The Thouless length $L_{\text{Th}}(t)$ in our simulations was derived as $L_{\text{Th}}(t) = L_{\text{int}}(t)/x$. Here, $L_{\text{int}}(t)$ denotes the system size at which the numerical estimation of the average of $\mathbb{E}[y]_{\text{sim}}(L = L_{\text{int}}(t), t)$ matches the theoretical prediction $\mathbb{E}[y]_{\text{RPM/BWM}}$ for a specific time t and value of x . The fact that the $L_{\text{Th}}(t)$ length estimates obtained by this procedure give close values for different x gives us strong confidence in the validity of the approach.

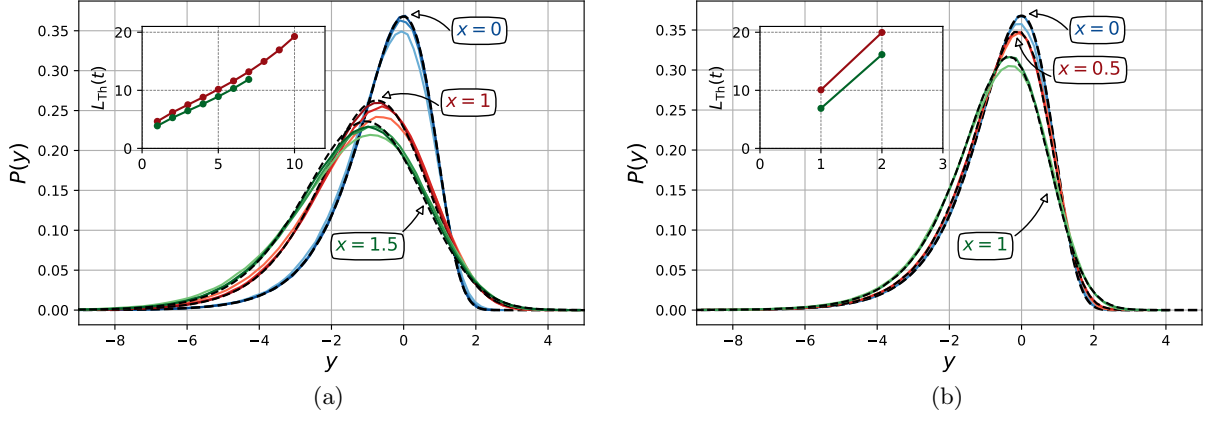


FIG. S1. Convergence of the numerical distributions (colored lines) to the theoretical ones (black-dashed line). (a): The obc numerical simulations of the RPM. For $x = 0$, we provide data for $(t, L) \in \{(10, 6), (15, 6), (20, 6)\}$; for $x = 1$, $(t, L) \in \{(3, 8), (5, 10), (10, 19)\}$; and for $x = 1.5$, $(t, L) \in \{(3, 10), (5, 13), (7, 18)\}$. (b): Pbc numerical simulations for the BWM at $q = 2$ and up to $L_{\text{max}} = 20$, $t_{\text{max}} = 20$. We provide data for $x = 0$ at $(t, L) \in \{(3, 15), (5, 15)\}$; for $x = 0.5$ at $(t, L) \in \{(1, 5), (2, 10)\}$; for $x = 1$ at $(t, L) \in \{(1, 7), (2, 16)\}$.

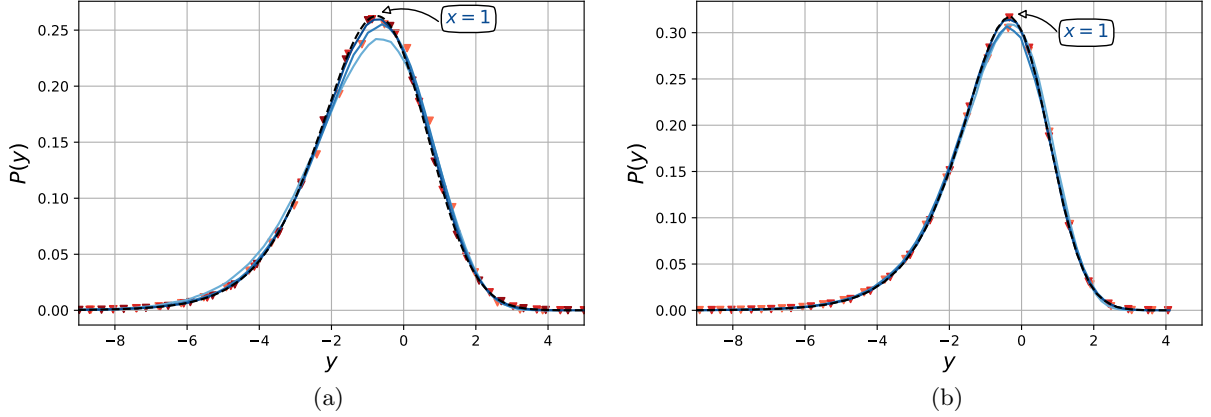


FIG. S2. Convergence of both of the RPM (blue curves) and BWM (coloured triangles) models to the same scaling limit (black dashed curve) for $x = 1$. (a) The obc numerical simulations of RPM at $(t, L) \in \{(3, 8), (5, 10), (10, 19)\}$ and of BWM at $(t, L) \in \{(1, 8), (3, 40), (4, 88)\}$; (b) The pbc numerical simulations of RPM at $(t, L) \in \{(3, 6), (5, 9), (10, 17)\}$ and of BWM at $(t, L) \in \{(1, 7), (2, 16)\}$.

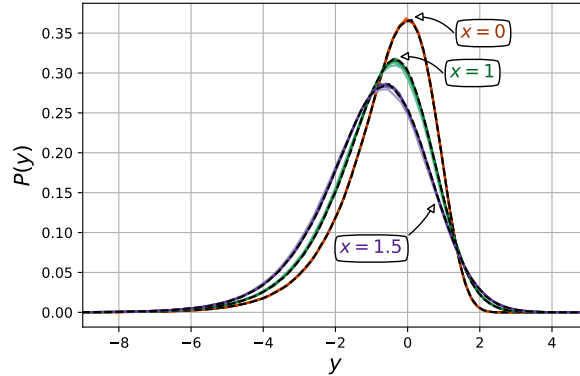


FIG. S3. The convergence in n for the pbc theoretical prediction on $P(y)$, generated using (12). The lines of the same colour correspond to $n = \{10, 25, 50, 100, 150\}$ from lighter to darker shade, with the black dashed line corresponding to $n = 300$.

2. Floquet circuits

Here we present our numerical findings concerning Floquet circuits, where the local gate $u_{j,j+1}(s) = u_{j,j+1}$ are independent of time step s for both the RPM and BWM models. Fig. S4 illustrates the convergence of the Floquet BWM to our theoretical predictions, while the Floquet RPM at $q = 2$ does not show convergence to our theoretical predictions. This observation aligns with prior works [33, 71], which suggests that the $q = 2$ Floquet RPM displays characteristics of a many-body localized (MBL) phase, except at large effective coupling ϵ . In the MBL, we do not expect the Thouless length to grow unbounded and exponentially fast with time t (see inset of Fig. S4(a)), thus invalidating the coarse-grained picture \tilde{G}_a of the transfer matrix in the spatial direction.

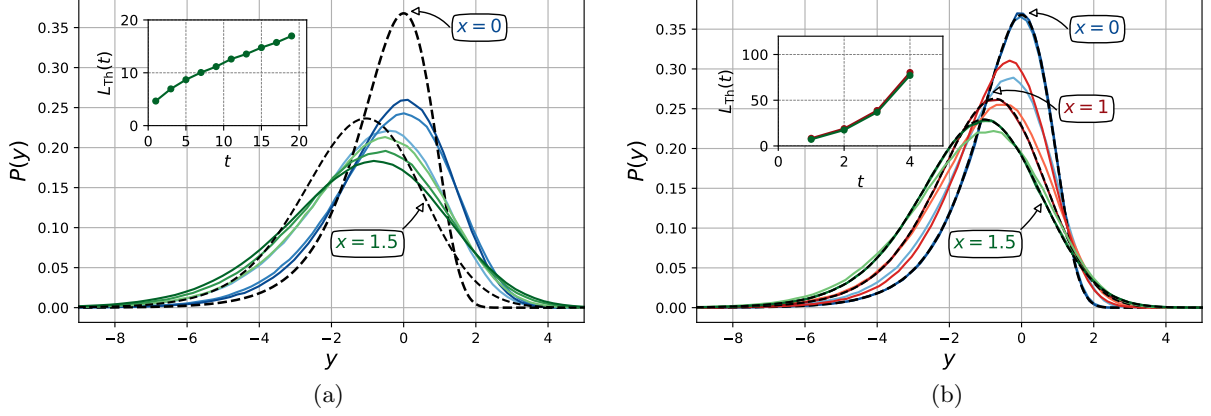


FIG. S4. The numerical distributions for the Floquet circuits (a): RPM with obc, $q = 2$, $\epsilon = 1$, $L_{\max} = 20$, and $t_{\max} = 20$. We present the distributions for $x = 0$ at $(t, L) \in \{(5, 8), (10, 8), (20, 8)\}$; for $x = 1.5$ at $(t, L) \in \{(11, 11), (13, 14), (15, 17)\}$. (b) BWM with obc, $q = 2$ for $x = 0$ at $(t, L) \in \{(1, 6), (3, 6), (5, 6)\}$; for $x = 1$ at $(t, L) \in \{(1, 8), (3, 19), (4, 80)\}$; for $x = 1.5$ at $(t, L) \in \{(1, 11), (3, 55), (4, 116)\}$.